Bulletin of the Seismological Society of America, Vol. 79, No. 6, pp. 1863–1882, December 1989

THE 1984 SOUTHERN YELLOW SEA EARTHQUAKE OF EASTERN CHINA: SOURCE PROPERTIES AND SEISMOTECTONIC IMPLICATIONS FOR A STABLE CONTINENTAL AREA

BY WAI-YING CHUNG AND BENJAMIN J. BRANTLEY

ABSTRACT

On 21 May 1984, a strong shock (M_S = 6.3, m_b = 5.7) occurred in the southern Yellow Sea which shook the densely populated coastal area of Eastern China. About 1 min before the main shock, a foreshock of m_b 5.4 occurred. Because of interference from the foreshock, no reliable *P*-wave first motions or focal mechanisms have been obtained for the main shock from local seismic data. In this paper, long-period teleseismic data have been used to investigate the source mechanism. Fault plane solutions determined from first motions as well as *P* and *SH* waveforms show a predominant strike-slip motion with a small dip-slip component on a steeply dipping plane. The tectonic environment of this event supports the observation that margins of former rifts tend to be sites of midplate seismic source regions. The Yellow Sea developed in a cratonic environment due to early Cenozoic rifting. The major graben faults strike NNE-SSW to NE-SW and are intersected by second-order faults trending WNW-ESE. Aftershock distribution suggests that the fault which generated the main shock probably strikes WNW-ESE. The mechanism determined in this paper strikes 120°, dips 88°, and slips 28°. This solution suggests that the earthquake ruptured along a secondary fault near the intersection of a more major NNE-SSW trending fault. The epicentral area is subject to to an ENE-WSW compression and a NNW-SSE extension. The seismic moment and focal depth are determined to be 1.09 × 10^{25} dyne-cm and 12 ± 4 km, respectively. Relative hypocentral locations indicate that the focal depth of the foreshock is similar to that of the main shock, and the hypocenter of the foreshock is located very close to the WNW-ESE striking nodal plane of the main shock mechanism and is about 20 km away from the main shock hypocenter.

Source properties of the southern Yellow Sea earthquake have been compared with those of three major earthquakes of North China. The stress drop of the Yellow Sea earthquake is determined to be about 42 bars. This value is much lower than the stress drops computed for the 1966 Hsingtai and the 1975 Haicheng earthquakes of North China. The southern Yellow Sea is characterized by short recurrence intervals, while the Hsingtai and Haicheng areas have very long recurrence intervals. The short recurrence intervals and low stress drop may reflect a lower material strength at the source region in the Yellow Sea.

INTRODUCTION

In spite of the considerable amount of work on intraplate earthquakes in the past 15 years (Sykes and Sbar, 1974; Kanamori and Anderson, 1975; Richardson and Solomon, 1976; Chen and Molnar, 1977; Tapponnier and Molnar, 1977; Sykes, 1978; Herrmann, 1979; Stein *et al.*, 1979; Liu and Kanamori, 1980; Okal, 1981; Chung, 1983; Johnston *et al.*, 1985; Ebel *et al.*, 1986; Talwani, 1986; Langston, 1987; Ma, 1987; among others), several problems remain, especially for those earthquakes in stable continental areas far away from plate margins. In many cases, the relationship between intraplate earthquakes and the subsurface seismogenic structure is not known. Because of low seismicity, the largest known earthquakes and recurrence intervals for a region are usually poorly known. This lack of information and understanding presents a challenge in seismotectonics and in seismic hazard evaluation. In the Central and Eastern United States, for example, two rare sequences of much interest to the American seismologists are the New Madrid earthquakes of 1811 and 1812 (Fuller, 1912; Nuttli, 1973; Johnston, 1982) and the Charleston earthquake of 1886 (Dutton, 1889). Unfortunately, both of these sequences are difficult to study because they occurred before the existence of any seismographs. Considerable uncertainty and ambiguity of the available data exist for these two earthquake sequences. Available data from other earthquakes in the Central and Eastern United States are very limited as well. As a result, controversies about the nature, the cause, and the associated seismic hazard in the regions remain unresolved. More study and more extensive comparison of intraplate earthquakes in stable continental areas worldwide will provide more insight and better understanding of the seismogenesis, earthquake characteristics, and seismic hazard of midplate earthquakes.

The southern Yellow Sea earthquake represents an intraplate event associated with a rifted continental margin and provides excellent opportunities for studying midplate earthquakes. On 21 May 1984, the coastal area of Eastern China, near the cities of Shanghai and Nantong, was strongly shaken by two earthquakes offshore. A foreshock, $m_b = 5.4$, occurred, followed approximately one min later by the main shock, $M_S = 6.3$ and $m_b = 5.7$, which took place in the southern part of the Yellow Sea (or Huang Hai) east of Jiangsu Province (Fig. 1). Even though the earthquakes only caused slight damage to buildings and minor casualties, the perceptible area on land was quite vast, including the Jiangsu Province and parts of Anhui, Zejiang, and Shandong Provinces. About 200 fishing boats in the Yellow Sea reported felt effects from the earthquakes.

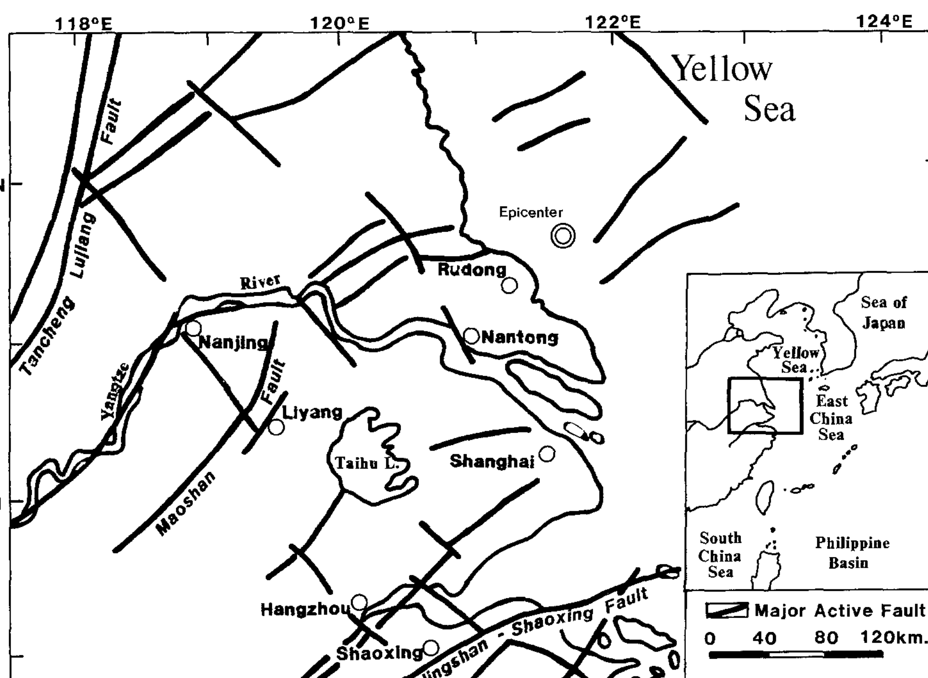

FIG. 1. The location of the southern Yellow Sea earthquake (the two concentric circles) and some related features in the southern Yellow Sea and the lower Yangtze river areas. Open circles represent major cities.

Swarms of microearthquakes and some foreshocks were reported to take place before the main shock (Cheng *et al.*, 1985; Li *et al.*, 1985; Zhang and He, 1986). Various precursory phenomena such as ground tilting, geomagnetic anomalies, water radon anomalies, chlorine content anomalies in wells, earth resistivity anomalies, and well water level variations were also reported in association with the earthquake (Ding *et al.*, 1985; Gao and Gu, 1985; Shen *et al.*, 1985; Wang and Xu, 1985; Zhang and He, 1986).

The focal mechanism of the foreshock was determined by Chinese seismologists using *P*-wave first motions from local and regional stations. However, due to the short time separation between the foreshock and the main shock, no reliable *P*-wave first motions of the main shock were obtained from most of these stations. As a result, the Chinese were unable to determine a fault plane solution for the main shock. On the basis of teleseismic data, three focal mechanisms were determined and reported in the *Preliminary Determination of Epicenters* (PDE). Unfortunately these three solutions are considerably different from each other and it is unclear which one of the three solutions is best. In this paper, long-period teleseismic *P* and *S* waves and some regional *P* waves from the main shock are studied to determine the focal mechanism, the source depth and duration, the seismic moment, and the stress drop. Teleseismic travel times of the foreshock and main shock are used to determine the relative location of the foreshock with respect to the main shock. The tectonic implications and stress drop of this earthquake are also discussed and compared with other major earthquakes in North China.

Seismological and Tectonic Settings

The southern Yellow Sea earthquake occurred in the southern Yellow Sea graben, slightly to the north of the outlet of the Yangtze River (Fig. 1). The epicentral area is located in a transition zone between the North and South China fault blocks. The North China fault block is characterized by high seismicity and extensively developed fault basins with normal right-lateral strike-slip faults trending NNE to NE. Secondary left-lateral strike-slip faults trend NW. The North China fault block is presently under extension with the least compressive stress oriented NW to NNW (Teng *et al.*, 1979; Zhang *et al.*, 1984). The South China fault block is characterized by much lower seismicity and fewer fault basins. NE-trending strike-slip faults with normal components are prevalent. The South China fault block has been compared to the Central and Eastern United States in terms of seismicity, geology, and tectonic settings (Johnston and Metzger, 1986; Ma, 1987).

Through most parts of China's earthquake history, the southern Yellow Sea area has been relatively seismically active in comparison with most other parts of the South China fault block, which is very stable. From 1764 to 1984, there have been 19 earthquakes with $M_S \geqq 6$, and 29 events with $6 > M_S \geqq 5$. The largest earthquake in the area had an $M_S = 6\frac{3}{4}$ to 7 and occurred in 1846 (Sun and Zhu, 1985). The last earthquake with $M_S > 6$, however, took place in 1927. The 21 May 1984 southern Yellow Sea event is the largest earthquake to have occurred in the area within the past 62 years.

Eastern China, which includes the North and South China fault blocks, is characterized by numerous rift basins associated with several epochs of rifting through the late Mesozoic and early Cenozoic. The Cretaceous marks a period of active rifting in the east. Rifting accelerated in the Tertiary producing graben-type basins trending NNE to NE through much of eastern and northern China (Ma and Wu, 1987). A later phase of rifting in the Tertiary resulted in regional subsidence and major downwarping along the pre-existing graben system. The basins of eastern and northern China today coincide with crustal thinning and a high heat flow (Ma and Wu, 1987). The driving mechanism of Eastern China's rifting is associated with the passive asthenospheric upwelling related to the westward subduction of the Philippine Sea and Pacific plates beneath the Asian plate (Juan, 1984).

The Yellow Sea developed entirely in a cratonic environment experiencing a series of extensional episodes during the early Tertiary resulting in the fragmentation of the craton into a number of intracratonic grabens. Granitic intrusions and thoelitic basalts are abundant throughout the basin. The Yellow Sea is separated from the East China Sea by the Neocathaysian massif (or Fukien-Reinan massif), which extends from continental southeastern China to south Korea (Fig. 2). This massif is composed of Precambrian and Mesozoic rocks and is a piece of detached basement resulting from mid to late Mesozoic rifting (Juan, 1984; Wageman *et al.*, 1970). The Yellow Sea is composed of three shallow basins separated by two low submarine ridges. These are bounded by major faults striking NE to NNE and secondary faults striking WNW to NW, with offsets being strike slip and dip slip. Since the late Cenozoic, differential vertical movement between faulted blocks has been taking place along high-angle faults associated with the horsts and grabens. Historical and recent earthquakes tend to occur along these faults (Qin, 1982). In

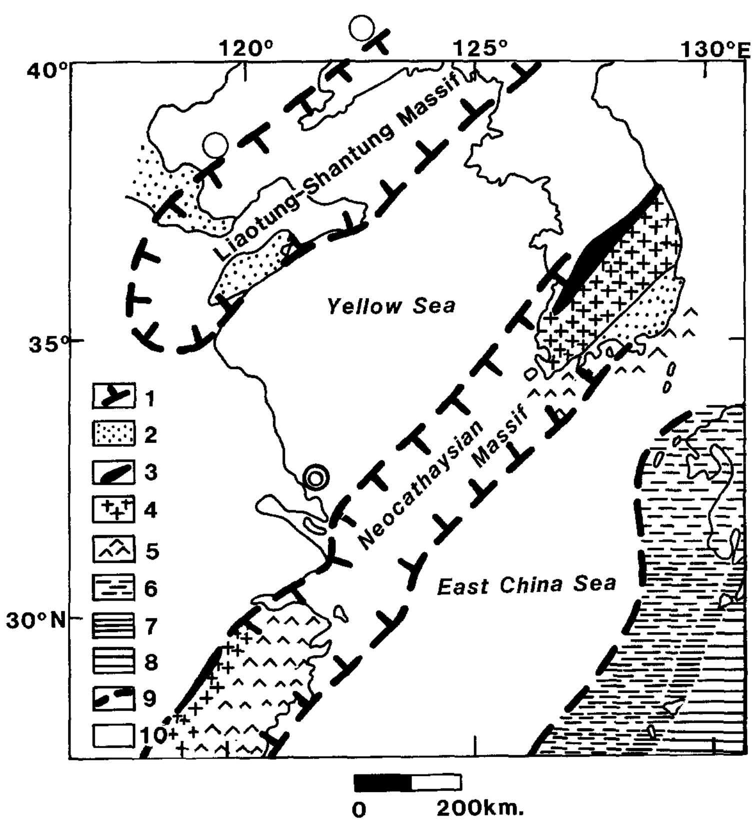

FIG. 2. Structural features of the Yellow Sea and the adjacent areas in the Upper Cretaceous. 1 = boundary of massif, 2 = depositional basins, 3 = mountain ranges, 4 = granitic rocks, 5 = volcanic rocks, 6 = shallow seas, 7 = geosynclinal areas, 8 = open sea, 9 = trace of limit of regression since Albian time, 10 = land areas (modified from Juan, 1984). The two concentric circles represent the epicenter of the 1984 southern Yellow Sea earthquake. The two open circles at the upper part of the figure are the epicenters of the 1969 Bo-hai Gulf and the 1975 Haicheng earthquakes.

this paper, we investigate how the 1984 southern Yellow Sea earthquake fits into the known tectonic picture for the region. Seismotectonic movement associated with this earthquake sequence will be compared and integrated with other geological evidence for a better understanding of Eastern China's tectonic model.

Hypocenters and Origin Times of the Main Shock and the Foreshock

A foreshock of $m_b = 5.4$ occurred at 15h37m52.2s UT located at 32.61°N and 121.60°E and at a focal depth of 31 km according to the International Seismological Center (ISC). The main shock, $M_S = 6.3$ and $m_b = 5.7$, took place at 15h39m0.7s UT; the epicenter was at 32.67°N, 121.51°E and the focal depth was 31 km. The focal depth of the foreshock was determined by Chinese seismologists at 17 ± 3 km. Cheng *et al.* (1985) did not determine the focal depth of the main shock, but, some Chinese seismologists considered that the main shock had the same focal depth as the foreshock (Zhang and He, 1986).

Focal Mechanism of the Main Shock and Distribution of Aftershocks

Even though the first motions of the main shock are masked by the foreshock at local and some regional distance, the teleseismic P-wave first-motion data are free from such interference and can be used. This is probably due to a combined effect of the Earth's filtering and the responses of the instruments involved. Another advantage of teleseismic data over regional data for this particular earthquake is a much better azimuthal coverage. Figure 3 presents the 22 P-wave first motions from long-period WWSSN and 13 (medium-period broadband) P-wave first motions at

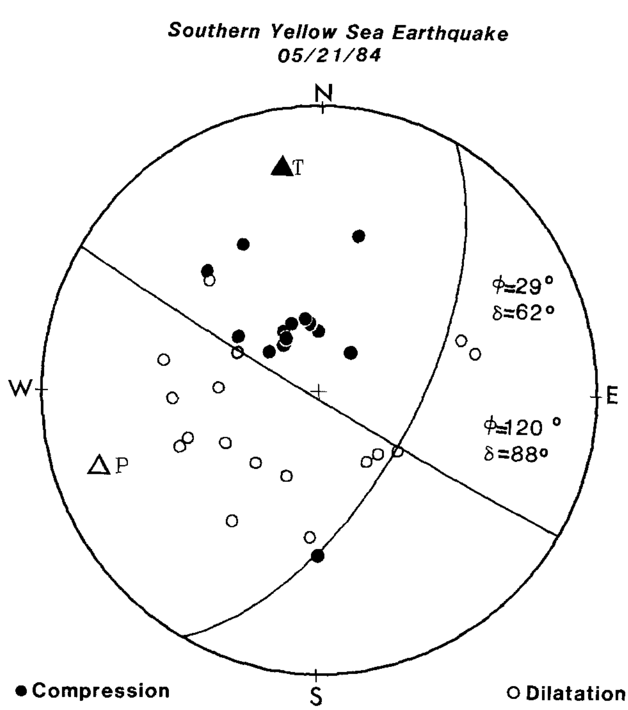

FIG. 3. P-wave first motions and focal mechanism of the southern Yellow Sea earthquake. Data are plotted using a lower hemisphere equal-area projection.

(relatively long range) regional distance from the Chinese standard seismic stations. The P-wave first motions alone cannot constrain the focal mechanism very well. The fault plane solution shown in Figure 3 is obtained with additional constraints from body-wave waveform modeling, as will be discussed later in this paper. The focal mechanisms of the foreshock and some large aftershocks were determined by Chinese seismologists using P-wave first motions (Cheng *et al.*, 1985) and are presented in Table 1 and Figure 9.

Since the area near the southern Yellow Sea had been considered seismically active, China established a local seismic network in the general area with more than 30 stations, located within 400 km of the main shock epicenter. Because the earthquake was offshore, the stations covered an azimuthal range less than 180° to the west of the epicenter. The characteristics of the southern Yellow Sea earthquake sequence have been studied by Cheng *et al.* (1985) and Zhang and He (1986). Figure 4 shows the epicentral distribution of the foreshock, main shock, and aftershocks which occurred within about 3 months after the main shock. The magnitude of the largest aftershock was $M_S = 4.9$. The difference in magnitude (M_S) between the main shock and the largest aftershock was 1.3. The southern Yellow Sea earthquake sequence appeared to form a foreshock-main shock-aftershock sequence. The b value was determined to be between 0.77 and 0.80. The aftershocks shown in Figure 4 approximately form an ellipse with a major axis of 30 km striking N30° to 45°W and a minor axis of 20 km. Based on this, the Chinese seismologists interpreted the fault plane of the main shock striking about NW. Most of the aftershocks were located to the northeast of the main shock. However, the variation of focal depths during the sequence was not resolved because of poor data quality (Cheng *et al.*, 1985; Zhang and He, 1986). In addition, most of these aftershocks are too small to be located using teleseismic data.

Relative Hypocentral Location of the Foreshock

In view of the poor azimuthal coverage of the local seismic stations and the problem of resolving the focal depths of different events in the earthquake sequence,

TABLE 1

Fault Plane Solutions of the Seven Largest Shocks in the Southern Yellow Sea Earthquake Sequence

Event	Date	M_s*	Strike	Dip	P axis		T axis	
					Azimuth	Plunge	Azimuth	Plunge
1	21 May 1984	5.7	257° 350°	60° 85°	217°	25°	119°	18°
2	21 May 1984	6.3†	29° 120°	62° 88°	251°	17°	348°	19°
3	22 May 1984	3.8	0° 96°	75° 70°	317°	25°	48°	4°
4	30 May 1984	3.7	12° 115°	75° 50°	68°	17°	324°	40°
5	7 June 1984	3.8	255° 350°	55° 81°	217°	29°	118°	18°
6	13 July 1984	3.9	45° 136°	55° 87°	265°	21°	6°	27°
7	23 July 1984	4.9	41° 135°	80° 67°	91°	9°	256°	23°

* The surface wave magnitudes of the foreshock and aftershocks are taken from Cheng *et al.* (1985).

† The M_S of the main shock is from ISC.

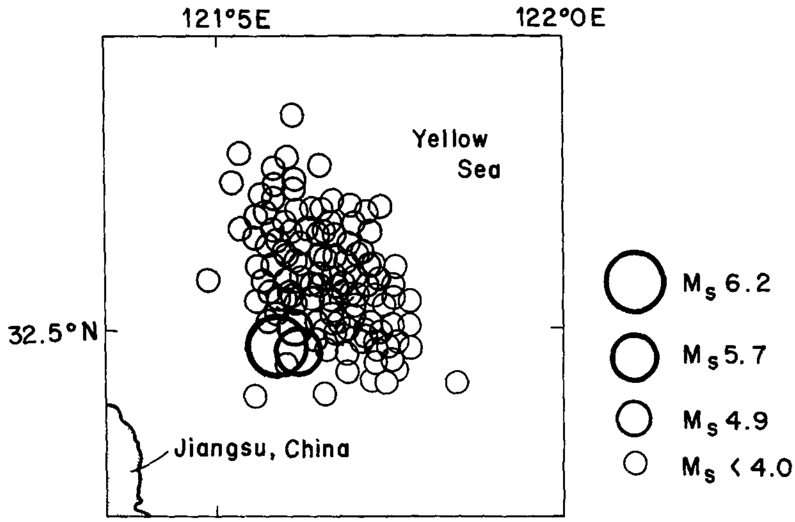

FIG. 4. Distribution of epicenters of the foreshock, the main shock, and the aftershocks (adapted from Cheng *et al.*, 1985).

a relative hypocentral location technique was employed to determine the location of the foreshock with respect to the main shock. The method described in Chung and Kanamori (1976) and Fukao (1972) has been used with the arrival time differences between the foreshock and the main shock reported in the ISC Bulletin. Consider the first earthquake (the main shock in this case) and the second earthquake (the foreshock) separated by ℓ km in distance and $\tau_{02} - \tau_{01}$ sec in origin time. The difference between arrival times of the first and the second P phases at the jth station, t_j^{12}, is approximately given by:

$$t_j^{12} = \tau_{02} - \tau_{01} - \frac{\ell}{v_p} \cos \delta_j \tag{1}$$

with

$$j = 1, 2, 3, \cdots$$

where δ_j is the angle between the line joining hypocenters 1 and 2 and the direction of P_1-wave radiation for the jth station and v_p is the P-wave velocity at the source. Both linear and nonlinear least squares methods can be applied to determine ℓ, $\tau_{02} - \tau_{01}$ and the azimuth and the plunge of the foreshock with respect to the main shock. Arrival times at 86 stations with epicentral distances greater than 10° and smaller than 90° have been used. Figure 5 shows the best linear least-squares fit of equation (1). For the convenience of analysis, the difference in arrival times in the plot has been shifted by an arbitrary amount. This is acceptable since we are mainly interested in determining the relative spatial relationship between the two events. Assuming $v_p = 6.0$ km/sec at the source, the foreshock is located at a distance of 19.66 km away from the main shock hypocenter and at an azimuth of 149° from north with respect to the main shock. The angle between the downward vertical and a line connecting the hypocenters of main shock and the foreshock is 90°. Thus, the foreshock has a focal depth about the same as the main shock. The 149° azimuth is consistent with the general trend of the aftershock distribution and is very close to the NW-striking nodal plane of the fault plane solution. This relative location result seems to favor the interpretation that the NW-striking nodal plane of the main shock is probably the fault.

Source Modeling from Teleseismic Body Waves

On the basis of teleseismic data, two focal mechanisms were determined and reported by the PDE and another mechanism was obtained by the Harvard University group. The three mechanisms, seismic moments, and the corresponding focal depths from the above studies are given in Table 2 and Figure 6. The two solutions from PDE are from P-wave first motions and moment-tensor inversion, respectively. The latter was based on P waveforms at 11 GDSN stations. However, the azimuthal coverage was not particularly good, with most of the stations concentrated to the NNE and NNW of the epicenter. In the present study, as will be shown later, we have much better azimuthal coverage with stations covering the SE, SW, and the west. The centroid-moment-tensor solution of Harvard was computed from GDSN data using normal mode theory. However, these three solutions differ considerably both in terms of fault-plane solution and focal depth. The reliability of results from

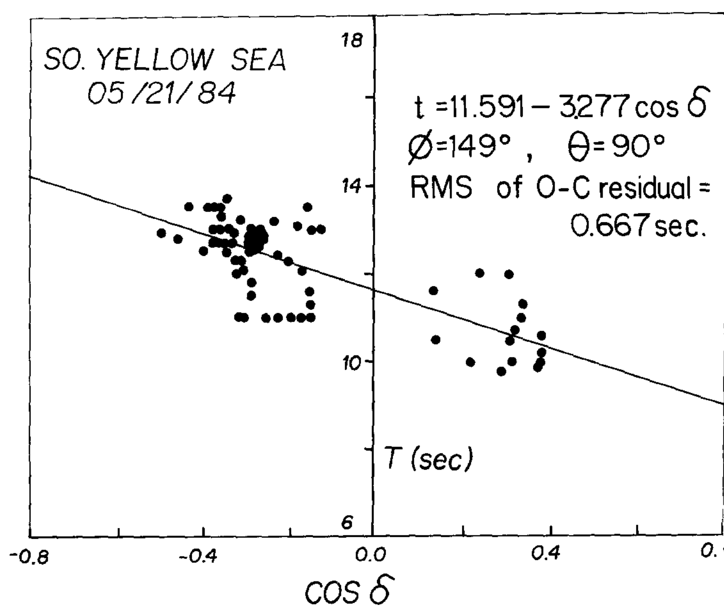

FIG. 5. A linear least-squares fit of the difference in P arrival times between the main shock and the foreshock.

TABLE 2

FOCAL MECHANISMS OF THE MAIN SHOCK REPORTED IN PDE

Solution	Method Used	Strike (°)	Dip (°)	Rake (°)	h (km)	Moment ($\times 10^{25}$ dyne-cm)
(a)	P-wave first motions	36	70	167	18	
		131	78	20		
(b)	Moment-tensor solution	106	67	24	6	1.3
		6	68	155		
(c)	Centroid moment-tensor solution	202	85	178	24.3	1.2
		292	88	5		

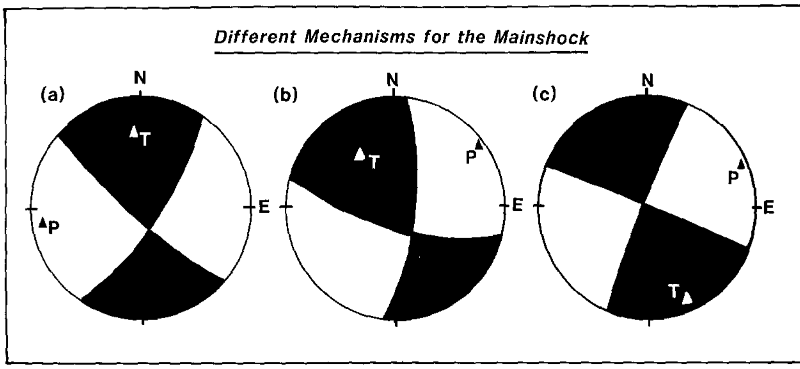

FIG. 6. Focal mechanisms of the main shock reported in PDE. (a) mechanism from P-wave first motions, (b) mechanism from moment-tensor solution, and (c) centroid-moment-tensor solution from Harvard.

source modeling or inversion can be quite dependent on station coverage (Satake, 1985) as well as source complexity (Scott and Kanamori, 1985). We evaluate the above solutions and determine the best solution of the earthquake using P- and S-wave data with a more extensive azimuthal coverage.

In addition to waveforms, P-wave first motions are also used to constrain the source mechanism. Nine P waveforms and ten SH waveforms from long-period WWSSN, one medium-period broadband P waveform from station KSH in China, and 35 P-wave first motions have been employed. The source model determined in this paper is based on simultaneously fitting the P and SH waveforms and first motions at all the available stations. Only stations in the distance range of 30 to 90° were used for the waveform study. The procedure for waveform data selection and processing is as described in Chung and Cipar (1983). We generated synthetic seismograms using the method described in Langston and Helmberger (1975) and Helmberger (1974). The far-field P-wave synthetic seismograms for a shear dislocation source in a half-space are constructed by adding three rays, P, pP, and sP, and convolving the summation with filters describing Earth attenuation, geometrical spreading, and instrument response. The values of t^* used in this paper are 1.0 sec for P waves and 4.0 sec for S waves. The P-wave velocities at the source are taken from the work by Teng *et al.* (1985), who studied the crustal velocity structures slightly to the south of the epicenter near Nantong, Shanghai (Fig. 1), and some adjacent areas using explosive sources and reflection and refraction techniques.

Observed and synthetic P waves for the southern Yellow Sea earthquake are shown in Figure 7; SH waves are shown in Figure 8. In deriving the best focal mechanism, we searched a very wide range in the parameter space. The neighborhoods of the solutions from Harvard and the PDE moment-tensor inversion of P waves were searched particularly well. Synthetics for numerous different starting models were computed and compared directly to the observed records. Models were then adjusted to get a best fit. The final model is shown in Figure 3. The first nodal plane has a strike of 120° ± 4° from the north, a dip angle of 88° ± 2° to the SW, and a slip angle of 28° ± 5°. The second nodal plane has a strike of 29° ± 4°, a dip angle of 62° ± 5°, and a slip angle of 178° ± 2°. If we interpret that the fault plane of the main shock strikes WNW on the basis of the trend of the aftershock distribution (Fig. 4), the motion at the source is left lateral on an almost vertical fault. Waveforms at each station provide significant constraints to the mechanism and the related source parameters. However, stations near the loop direction of the

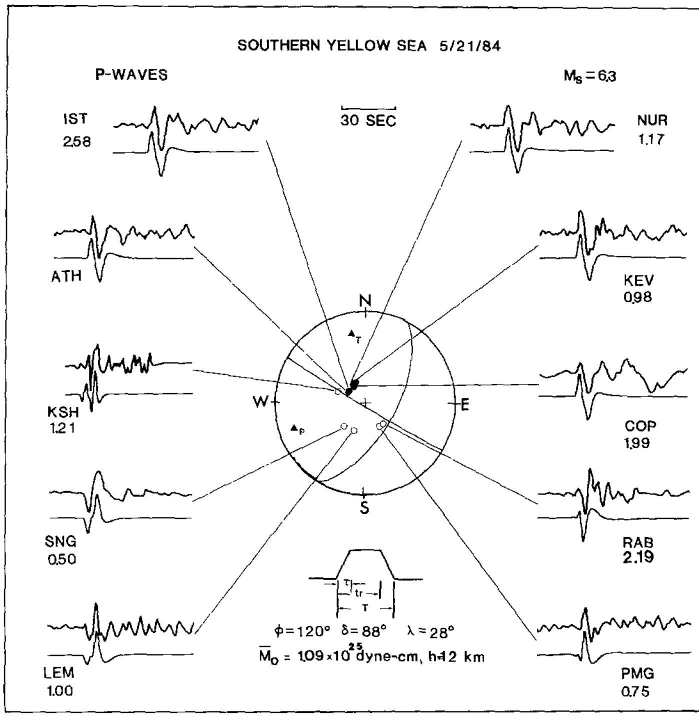

FIG. 7. Comparison of observed (upper trace) and synthetic (lower trace) P waves of the 21 May 1984 southern Yellow Sea earthquake. The far-field source-time function used is trapezoidal with a rise time τ, a rupture time t_r, and a total duration T. Fault strike (ϕ), dip (δ), slip angle (λ), source depth (h) and average moment ($\bar{M}_0$) are also indicated. Number by the side of synthetic trace is the seismic moment at that station.

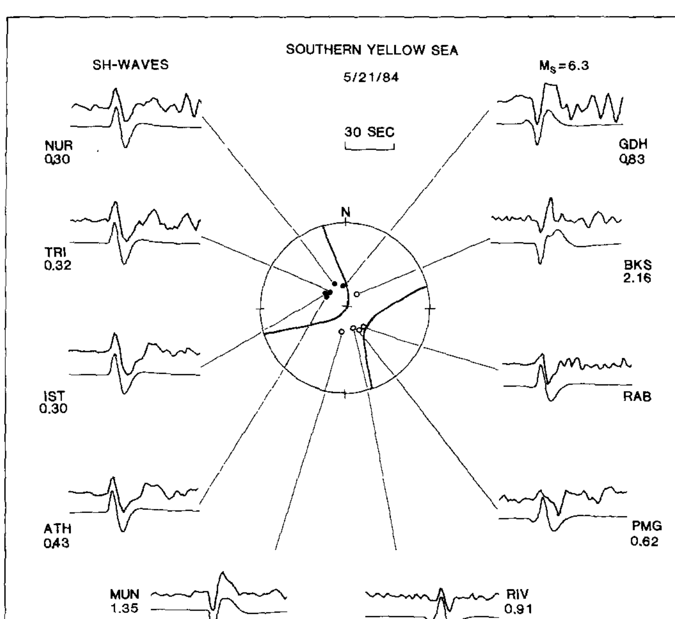

FIG. 8. Comparison of observed (upper trace) and synthetic (lower trace) SH waves of the southern Yellow Sea earthquake. Number by the side of synthetic trace is the seismic moment at that station.

radiation pattern are not very sensitive to subtle changes or certain changes of the focal mechanism. On the other hand, stations near the nodal planes are much more sensitive to the fault orientation. For obtaining tight constraints to the fault plane solution, waveforms of the near nodal stations (e.g., KSH, PMG, and RAB) should be matched well by the synthetics whenever possible. As we can see from Figures 7 and 8, in general, the agreement between observed and synthetic seismograms is excellent. As a result, the focal mechanism is strongly controlled by the nodal stations in addition to the non-nodal ones.

For shallow earthquakes, the observed *P* waveform at a station is actually the sum of *P*, *pP*, and *sS*; similarly the *SH* waveform is the sum of *S* and *sS*. Hence, a station at a nodal direction of *P* or *S* may not be located at the nodal direction of the depth phases. Consequently, the amplitude of the observed *P* or *S* waveforms at a nodal station of *P* or *S*, in many cases, is not small, and can be used to estimate seismic moment if the match between the observed and the synthetic traces are reasonable and the seismic moment derived does not have large deviation compared with those from other stations. In our computation of seismic moment, stations with large deviation or unstable estimates of seismic moment are excluded. For this reason, the *P* wave of station ATH and the *SH* wave of RAB were not used for computing seismic moment. The seismic moments from *P* and *SH* waves are 1.59×10^{25} dyne-cm and 0.80×10^{25} dyne-cm, respectively. The average seismic moment, $\bar{M}_0$, from both *P* and *SH* waves is 1.09×10^{25} dyne-cm which is slightly smaller than those from the Harvard centroid-moment-tensor solution and the PDE moment-tensor solution. The trapezoidal far-field source-time function has a rise time, τ, of 1.1 sec and a rupture time, t_r, of 1.3 sec (Fig. 7). The focal depth given by the ISC was 31 km. However, the time separation between the direct *P* and the depth phases revealed this to be too deep. Depths of 24 km and 18 km from Harvard and PDE also appeared to be too large to interpret the body wave waveforms. A depth of 12 ± 4 km was determined through the waveform modeling, which falls between the depth of 17 ± 3 km determined for the foreshock by Chinese seismologists and the depth of 6 km reported by PDE from the moment-tensor solution.

As mentioned earlier, the focal mechanism of the main shock could not be determined from the *P*-wave polarities at most of the local and regional distances. Interpretations regarding the main shock were made by some Chinese seismologists based on the assumption that the main shock and the foreshock had similar mechanisms. Comparing the aftershock distribution (Fig. 4) with the focal mechanism of the foreshock (Mechanism 1, Fig. 9), Cheng *et al.* (1985) picked the NNW-striking nodal plane of the foreshock as the fault of the main shock and suggested the fault motion was right lateral. In our waveform modeling, we used the focal mechanism of the foreshock to generate synthetic seismograms but the synthetics could not fit the observed waveforms of the main shock. The mechanism which best fit the main shock waveforms (Figs. 3 and 7) differs significantly from that of the foreshock. If we pick the WNW-striking nodal plane as the fault, as Cheng *et al.* (1985) did, the fault motion associated with the main shock is left lateral based on the results from this study. Since the aftershock zone does not define a very sharp and linear feature striking WNW, the possibility that the NNE-striking nodal plane is the fault plane for the main shock cannot be completely ruled out. However, the relative location of the foreshock being to the SE of the main shock and the NW elliptical trend of the aftershock zone lead us to favor the WNW-striking nodal plane of the main shock mechanism as the fault plane.

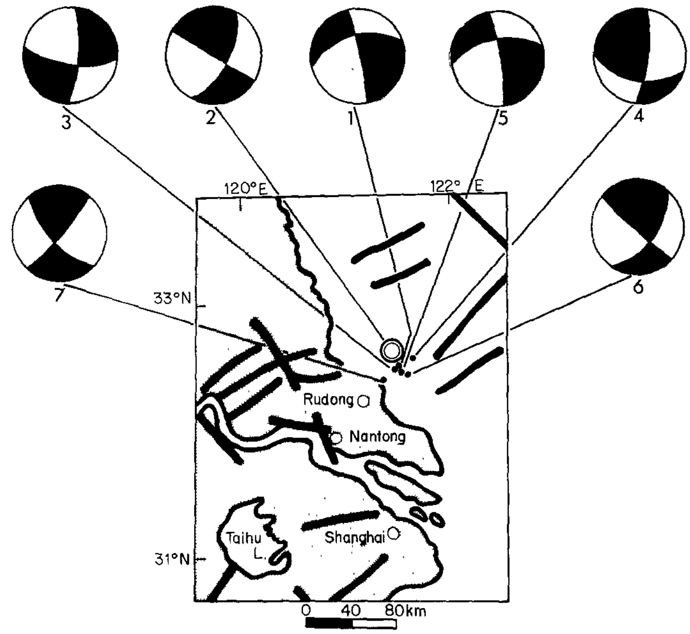

FIG. 9. Focal mechanisms of the foreshock (event 1), the main shock (event 2), and five major aftershocks (events 3 to 7) of the southern Yellow Sea sequence. See Table 1 for the parameters of the fault plane solutions.

FAULTING MECHANISMS OF THE SOUTHERN YELLOW SEA SEQUENCE

The fault plane solutions of the foreshock, the main shock, and the five largest aftershocks are plotted on a map (Fig. 9). All these solutions (Table 1) have a large strike-slip component and at least one nearly vertical nodal plane. In spite of these similarities, it is difficult to find a simple model to explain the tectonic movement at the source region because of significant variations among the focal mechanisms. As mentioned earlier, the focal mechanism of the main shock (event 2) is not the same as that of the foreshock (event 1). Note the similarities between events 1 and 5 and between events 6 and 7. However, the focal solutions of events 1 and 5 are different from those of events 6 and 7, which are two aftershocks at a later stage of the sequence. The mechanism of event 3 is especially different from the rest. It has been explained as a rebound of the fault block following a local overshoot associated with the main shock (Cheng *et al.*, 1985). The variation of the focal mechanisms may be due to uncertainty associated with the solutions. It also indicates the complexity of the rupture process as well as that of the fault geometry and distribution. From the local geology, as mentioned earlier, it is known that there are major NE-trending faults in the area. Combining this with the trend of aftershock distribution and the epicentral locations of the earthquake sequence, it is very likely that the earthquake sequence occurred near the intersection of two sets of faults which strike more or less NE and NW, respectively. If the epicentral locations of the major aftershocks in Figure 9 are reliable, some of the aftershocks probably also ruptured the NNE-striking faults in the area. The slightly diffused distribution of epicenters of this earthquake sequence can be interpreted as the following. During the earthquake sequence, both the WNW-striking and the NNE-striking planes were ruptured with a major rupture along the former one and a relatively minor rupture on the later one. In order to explain the observed variation of fault plane solutions, each set of the intersecting faults probably needs to bend or change strike direction in the aftershock area.

Source Parameters and Stress Drop

We can also estimate source parameters such as fault area, average dislocation, and average stress drop by making some assumptions. The extent of the aftershock activity immediately after the main shock (hours or days), in some cases, has been used to estimate the fault area (Ben-Menahem and Toksöz, 1963; Kanamori, 1970; Kanamori and Anderson, 1975). However, for the southern Yellow Sea earthquake, detailed aftershock data are not available. The aftershock distribution in Figure 4 was from a period of about 3 months. The aftershock area shown is probably much larger than the fault area during the main shock rupture. In this paper, we estimate the source dimensions from the total duration of the far-field source-time function.

Assume that the rupture initiates at a point and then spreads out in every direction on the fault plane with a constant rupture velocity. Making the approximation that the radius of the circular fault is proportional to the product of the rise time and the shear-wave velocity β at the source (Geller, 1976), the fault radius a is given by

$$a = \frac{28\pi\beta T}{35\pi + 16.17\pi \sin \delta + 64}$$

where T is the total duration of the far-field source-time function and δ is the angle between the normal to the fault plane and the P-ray direction (Chung and Cipar, 1983; and Ebel *et al.*, 1978). Using $T = 3.5$ sec from waveform modeling, we have $a = 4.84$ km and fault area $A = 73.5$ km^2. We can compute the average dislocation $\bar{D}$ from the relation $\bar{D} = M_0/\mu A$ where M_0 and μ are seismic moment and rigidity, respectively. We obtain a $\bar{D} = 43.5$ cm if a $\mu = 3.4 \times 10^{11}$ dyne-cm^{-2} is used. The average dislocation velocity, which is given by $\dot{\bar{D}} = \bar{D}/\tau$, equals 39.5 cm/sec. Assuming $\lambda = \mu$, we have a stress drop

$$\Delta\sigma = \frac{7\pi\mu\bar{D}}{16a}$$

and $\Delta\sigma = 42.1$ bars. The strain drop, $\Delta\epsilon = \Delta\sigma/\mu = 1.238 \times 10^{-4}$. The strain energy released, $W = (\Delta\sigma M_0)/2\mu = 6.747 \times 10^{20}$ erg, assuming the residual stress after faulting is zero.

Comparison with Other Intraplate Earthquakes

The southern Yellow Sea earthquake shares several similarities with some other major earthquakes in North China. From the focal mechanism solution of the southern Yellow Sea earthquake (Fig. 3), the azimuths of the compressive and tensile axes are at N109°W and N12°W, respectively, and their correspondent plunges are 17° and 19°, respectively. The focal region is under an almost horizontal compressional stress in the ENE-WSW direction and an extensional stress in the NNW-SSE direction. This stress orientation is very similar to the 1966 Hsingtai (or Xingtai) earthquake ($M_S = 7.2$), the 1969 Bo-hai Gulf earthquake ($M_S = 7.4$), and the 1975 Haicheng earthquake ($M_S = 7.3$) in North China (Fig. 10) (Gu *et al.*,

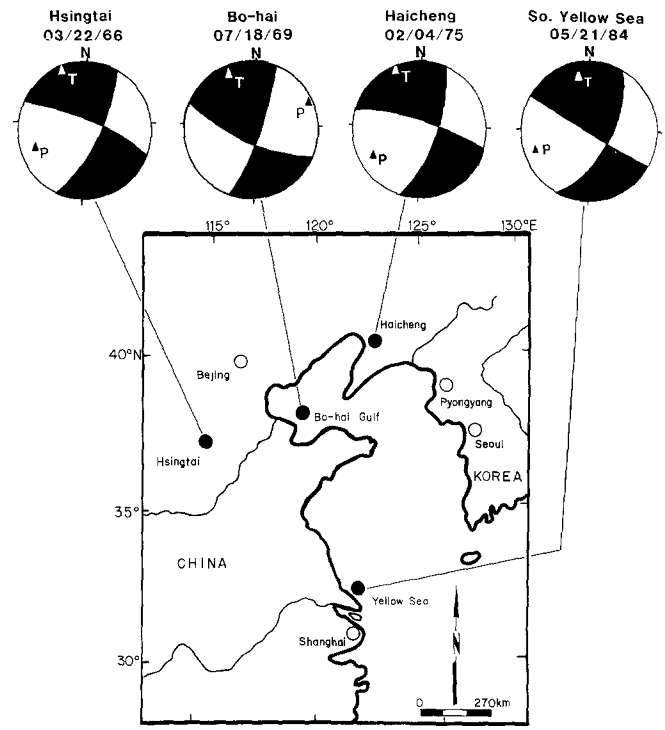

FIG. 10. Locations and focal mechanisms of the 1984 southern Yellow Sea, the 1966 Hsingtai, the 1969 Bo-hai Gulf, and the 1975 Haicheng earthquakes in Eastern China.

1976; He and Xie, 1977; Cipar, 1979; Ma *et al.*, 1982; Chung and Cipar, 1983; Chung, 1983). The focal mechanisms of the above earthquakes are given in Table 3.

The major faults in the southern Yellow Sea and adjacent area strike NE to NNE. The main shock of the southern Yellow Sea earthquake, however, probably ruptured along a WNW-striking secondary fault near its intersection with a first-order NE- to NNE-striking fault. This situation is similar to the 1975 Haicheng earthquake (Hsu, 1976; Ma *et al.*, 1982). For the 1966 Hsingtai earthquakes, the overall aftershock distribution ran NNE, while the individual aftershock distributions of the four major shocks ($M_S > 6$) follows a WNW trend, suggesting rupture along secondary faults near intersections with first-order faults (Ma *et al.*, 1982). The 1969 Bo-hai Gulf earthquake also occurred near an intersection of a NE-striking fault and a WNW-striking fault. The Bo-hai Gulf event is not so well studied because it occurred offshore; however, it has been suggested that the rupture was along a WNW fault (Molnar and Deng, 1984).

The Haicheng earthquake had a number of precursory anomalies and was predicted by the Chinese (Scholz, 1977). The southern Yellow Sea earthquake also had several precursors. Foreshocks were reported to occur prior to the Haicheng, Hsingtai, and the southern Yellow Sea earthquakes. For the Haicheng earthquake, foreshock activity played a very important role in terms of short term prediction.

The 1984 southern Yellow Sea earthquake took place slightly to the NW of the Neocathaysian massif. Interestingly, the 1969 Bo-hai Gulf and the 1975 Haicheng earthquakes also occurred near the northwestern edge of the Liaotung-Shantung massif which is parallel to the Neocathaysian massif (Fig. 2). Both the Yellow Sea and North China regions have experienced tensional activity and subsidence in

TABLE 3

FAULT PLANE SOLUTIONS OF THREE MAJOR EARTHQUAKES IN NORTH CHINA

Event	Date	Strike (°)	Dip (°)	Rake (°)	h (km)
Hsingtai	22 March 1966	26	73	191	9
		292	79	−18	
Bo-hai Gulf	18 July 1969	20	80	165	35
		112	75	10	
Haicheng	4 February 1975	21	72	192	10
		288	78	342	

their tectonic history and share several similarities in geology (Juan, 1984), which may explain the similarities of seismic characteristics among these four Chinese earthquakes.

On the other hand, several significant differences also exist among the southern Yellow Sea earthquake and the other three Chinese earthquakes mentioned above. The source parameters of the southern Yellow Sea earthquake and some other midplate earthquakes, studied by Chung and Cipar (1983), are given in Table 4. The parameters in this table, which were all determined by using similar waveform modeling or inversion techniques, and the stress drops were computed using the same method as described above. In this way, we minimize model dependence and have a more meaningful comparison. Among the Hsingtai, the Haicheng, and the southern Yellow Sea earthquakes, the smallest M_S and the lowest stress drop correspond to the southern Yellow Sea earthquake. The stress drop of the Haicheng event (144 bars) was almost three times as high as that of the southern Yellow Sea event, and the two largest shocks of the Hsingtai sequence (112 bars and 194 bars) are about two to four times higher. The stress drops of the 15 midplate earthquakes studied by Chung and Cipar (1983) vary from 18 bars to 894 bars with a median of 144 bars. Kanamori and Anderson (1975) obtained an average stress drop of about 100 bars from intraplate events near plate boundaries. Hence, the stress drop of the southern Yellow Sea earthquake appears to be much lower than that of the average intraplate events.

Although the largest known earthquake in the southern Yellow Sea area is not very large ($M_S = 6\frac{3}{4}$ to 7) the seismicity there is relatively active. Sun and Zhu (1985) employed a method described in Molnar (1979) to study the earthquake recurrence intervals in the southern Yellow Sea. The recurrence intervals for events with M_S $6\frac{3}{4}$, $6\frac{3}{4}$, and 7 are found to be approximately 27 yr, 38 yr, and 44 yr, respectively. These recurrence intervals may have some uncertainty (because some empirical relationships are used) but clearly indicate very short repeat times for the intraplate earthquakes in the area. For the Haicheng area, there were no known earthquakes in Chinese history with $M_S \geqq 7$ before the 1975 ($M_S = 7.3$) earthquake. The recurrence interval of $M_S \geqq 7$ earthquakes is probably larger than 1500 to 2000 yr. For the Hsingtai area, the recurrence interval of $M_S \geqq 7$ earthquakes is also very large. It is probably larger than 1670 to 2000 yr (Chung, 1983; Ku, 1983; Xie, 1983; Xie and Qai, 1985).

For these three earthquakes, there seems to be a correlation between the stress drop and the recurrence interval. The Hsingtai and Haicheng earthquakes have stress drops much higher than that of the southern Yellow Sea event. Correspondingly, the maximum magnitudes are greater and the recurrence intervals are

TABLE 4

SOURCE PARAMETERS AND STRESS DROPS OF 16 INTRAPLATE EARTHQUAKES

Event	Date	Location	Depth (km)	m_b	M_s	Moment ($\times 10^{25}$ dyn-cm)	Stress Drop (bars)
1	21 May 1984	32.7 N 121.5 E So. Yellow Sea, China	12	5.7	6.3	1.09	42.1
2	7 March 1966	37.4 N 114.9 E Hsingtai, China	10	5.6	6.8	8.32	111.8
3	22 March 1966	37.5 N 115.1 E Hsingtai, China	9	5.6	6.7	2.97	52.7
4	22 March 1966	37.5 N 115.1 E Hsingtai, China	9	5.9	7.2	15.12	193.7
5	26 March 1966	37.5 N 115.3 E Hsingtai, China	15	5.2	6.2	1.43	53.5
6	4 September 1963	71.3 N 73.0 W Baffin Island, passive continental margin	7	5.9	6.2	1.7	222.5
7	23 October 1964	19.8 N 56.0 W East of West Indies, Atlantic Ocean	23	6.4	6.3	6.2	893.5
8	16 April 1965	64.7 N 160.1 W Back arc, Alaska	12	5.8		1.3	67.0
9	12 September 1965	6.5 S 70.8 E Chagos-Laccadive ridge, Indian Ocean	15	6.2	6.0	3.5	213.0
10	7 October 1965	12.5 N 114.5 E South China Sea	5	5.9	5.6	1.	18.0
11	12 September 1966	39.4 N 120.2 W Truckee, California	10	5.7	5.9	0.83	79.9
12	10 December 1967	17.5 N 73.8 E Koyna, India	4.5	6.0	6.5	3.2	20.1
13	24 March 1970	21.9 S 126.6 E Continent, Australian Plate	12.	5.9	1.4	2.5	176.5
14	30 September 1971	0.4 S 4.7 W Atlantic Oceanic, African Plate	13.	6.0	5.5	0.7	397.5
15	4 February 1975	40.7 N 122.8 E Haicheng, China	10.	6.4	7.3	30.	143.7
16	24 March 1978	29.9 N 673. W Bermuda, Atlantic Ocean	11	6.1	5.8	3.4	206.9

considerably longer in the Hsingtai and Haicheng areas than in the southern Yellow Sea. Kanamori and Allen (1986) studied the source parameters of 26 crustal earthquakes over a wide range of repeat times and found that the earthquakes with long repeat times have higher average stress drops than those with short repeat times. The correlation observed in the present study is consistent with their results. This observed relationship between earthquake repeat time and stress drop probably has to do with stress-drop dependence on long-term slip rate, healing effect on the fault plane, and inherent difference in fault strength or material properties in the source region (Kanamori and Allen, 1986; Cao and Aki, 1986).

The southern Yellow Sea is a highly fractured area with the NW- and NE-striking faults being remnants of previous rifting in the area. These faults have been reactivated by the present-day tectonic stresses, and it appears that the source region is incapable of withstanding a high stress level. Hence, earthquakes with low stress drop, low magnitude, and short recurrence intervals may be intrinsic of low shear and frictional strengths of the source region.

CONCLUSIONS

The southern Yellow Sea earthquake is an example of a midplate earthquake occurring near the margin of a former rift. It took place as a foreshock-main shock-aftershock sequence. The major graben faults strike NNE-SSW to NE-SW and are intersected by second-order faults trending WNW-ESE. The earthquake probably ruptured along a secondary fault near the intersection of a NNE-SSW-trending fault. If so, the fault motion for the main shock was left-lateral strike slip on an almost vertical plane with mechanism: strike 120°, dip 88°, and rake 28°. The faulting mechanism of the entire sequence, however, shows a complex pattern, indicating movements on multiple faults or both sets of intersecting faults which probably bend slightly or change strike directions in the area. The epicentral area is subject to an ENE-WSW compression and a NNW-SSE extension which is consistent with the tectonic stress orientation in the general area. The seismic moment and focal depth of the main shock are determined to be 1.09×10^{25} dyne-cm and 12 ± 4 km, respectively. Results of relative hypocentral location indicate that the foreshock, which occurred about 1 min before the main shock, has a focal depth approximately the same as the main shock and is about 20 km to the SE of the main shock.

The probability of the southern Yellow Sea earthquake having ruptured a secondary fault is not unique to Eastern China. Something similar occurred in the 1966 Hsingtai, the 1969 Bo-hai Gulf, and the 1975 Haicheng earthquakes. The earthquakes ruptured along WNW-striking faults even though the major faults strike NNE to NE. The stress drop of the southern Yellow Sea earthquake is determined to be about 42 bars which, in comparison to the 1966 Hsingtai and the 1975 Haicheng earthquakes, appears to be much lower. The southern Yellow Sea is characterized by short recurrence intervals while the Hsingtai and Haicheng areas have very long recurrence intervals. The short recurrence intervals and low stress drop may reflect a lower material strength at the source region in the southern Yellow Sea. This study presents an example of regional variation in earthquake source parameters and characteristics in Eastern China.

ACKNOWLEDGMENTS

We would like to thank John Cipar and José Pujol for critically reading the manuscript and providing suggestions for improvements. Helpful comments from David M. Boore and Francis T. Wu are also appreciated. The manuscript was carefully typed by Sandra Early. The figures were skillfully drafted by Tanya George. This research was supported by the State of Tennessee Centers of Excellence Program and also in part by the Division of Earth Science, National Science Foundation, NSF Grant EAR-8817449 and Electric Power Research Institute, Inc. Contract RP 2556-54.

REFERENCES

Ben-Menahem, A. and M. N. Toksöz (1963). Source mechanism from spectra of long-period surface waves, *J. Geophys. Res.* **68,** 5207–5222.

Cao, T. and K. Aki (1986). Effect of slip rate on stress drop, *Pure Appl. Geophys.* **124,** 515–529.

Chen, W. P. and P. Molnar (1977). Seismic moments of major earthquakes and the average rate of slip in central Asia, *J. Geophys. Res.* **82,** 2945–2969.

Cheng, D., H. Xie, C. Wang, C. Yang, and W. Huang (1985). Characteristics of the earthquake sequence of *M* 6.2 in South Yellow Sea, *Earthquake* **1,** 25–31 (in Chinese).

Chung, W.-Y. (1983). Mode of strain release in three graben-associated earthquakes, *Tectonics* **2,** 379–398.

Chung, W.-Y. and H. Kanamori (1976). Source process and tectonic implications of the Spanish deep-focus earthquake of March 29, 1954, *Phys. Earth Planet. Interiors* **13,** 85–96.

Chung, W.-Y. and J. J. Cipar (1983). Source modeling of the Hsingtai, China earthquakes of March 1966, *Phys. Earth Planet. Interiors* **33,** 111–125.

Cipar, J. (1979). Source processes of the Haicheng, China earthquake from observations of *P*- and *S*-waves, *Bull. Seism. Soc. Am.* **69,** 1903–1916.

Ding, J., X. Huang, and S. Zhang (1985). Geomagnetic anomalies before the Wunansha earthquake ($M = 6.2$) in the south of the Huanghai Sea, *Northwestern Seism. J.* **7,** 104–105 (in Chinese).

Dutton, C. E. (1889). The Charleston earthquake of August 31, 1886, *U.S. Geol. Surv. Ninth Ann. Rept., 1887–88,* 203–528.

Ebel, J. E., L. J. Burdick, and G. S. Stewart (1978). The source mechanism of the August 7, 1966 El Golfo earthquake, *Bull. Seism. Soc. Am.* **68,** 1281–1292.

Ebel, J. E., P. E. Somerville, and J. D. McIver (1986). A study of the source parameters of some large earthquakes of northeastern North America, *J. Geophys. Res.* **91,** 8231–8247.

Fukao, Y. (1972). Source process for a large deep-focus earthquake and its tectonic implications—the western Brazil earthquakes of 1963, *Phys. Earth Planet. Interiors* **5,** 61–76.

Fuller, M. L. (1912). The New Madrid earthquake, *U.S. Geol. Surv. Bull.* **494,** 119 pp.

Gao, H. and X. Gu (1985). Anomalous tilt at Changshu seismic station before the South Yellow Sea *M* 6.2 earthquake of May 21, 1984, *Earthquake* **4,** 13–18 (in Chinese).

Geller, R. J. (1976). Scaling relations for earthquake source parameters and magnitudes, *Bull. Seism. Soc. Am.* **66,** 1501–1523.

Gu, H., Y. T. Chen, X. Gao, and Y. Zhao (1976). Focal mechanism of Haicheng, Liaoning province, earthquake of February 4, 1975, *Acta Geophys. Sin.* **19,** 270 (in Chinese).

Helmberger, D. V. (1974). Generalized ray theory for shear dislocations, *Bull. Seism. Soc. Am.* **64,** 45–64.

Herrmann, R. B. (1979). Surface wave focal mechanisms for eastern North American earthquakes with tectonic implications, *J. Geophys. Res.* **84,** 3543–3552.

He, Z.-T. and T. Xie (1977). The hypocentral distribution of the Hsingtai earthquake series, tectonic stress field and the process of earthquake occurrences, *Acta Geophys. Sin.* **20,** 131–142.

Hsu, S. H. (1976). Characteristics of the Haicheng earthquake of 1975, in *Proceedings of the Lectures by the Seismological Delegation of the People's Republic of China,* Paul M. Muller (Editor), Jet Propul. Lab., Calif. Inst. of Technol., Pasadena.

Johnston, A. C. (1982). A major earthquake zone on the Mississippi, *Scientific American* **246,** 60–68.

Johnston, A. C. and A. G. Metzger (1986). The seismicity of stable continental interiors, *Tennessee Earthquake Information Center Special Report* **86-1,** Vol. 1 and Vol. 2.

Johnston, A. C., D. J. Reinbold, and S. I. Brewer (1985). Seismotectonics of the southern Appalachians, *Bull. Seism. Soc. Am.* **75,** 291–312.

Juan, V. C. (1984). Thermal-tectonic evolution of Yellow-Sea and East China Sea—implication of transformation of continental to oceanic crust and marginal basin formation, *Tectonophysics* **125,** 231–244.

Kanamori, H. (1970). Synthesis of long-period surface waves and its application to earthquake source studies—Kurile Islands earthquake of October 13, 1963, *J. Geophys. Res.* **75,** 5011–5027.

Kanamori, H. and C. R. Allen (1986). Earthquake repeat time and average stress drop, in *Earthquake Source Mechanics,* S. Das, J. Boatwright, and C. H. Scholz (Editors), American Geophysical Union Monograph **37,** 227–235.

Kanamori, H. and D. L. Anderson (1975). Theoretical basis of some empirical relations in seismology, *Bull. Seism. Soc. Am.* **65,** 1073–1095.

Ku, K.-H. (1983). *A Catalog of Earthquakes in China,* Science Press, Beijing (in Chinese).

Langston, C. A. (1987). Depth of faulting during the 1968 Meckering, Australia, earthquake sequence determined from waveform analysis of local seismograms, *J. Geophys. Res.* **92,** 11561–11574.

Langston, C. A. and D. V. Helmberger (1975). A procedure for modeling shallow dislocation sources, *Geophys. J.* **42,** 117–130.

Li, Y., J. Lin, and F. Lin (1985). Seismicity skeleton in and around North China and precursory phenomena occurred before ten earthquakes since 1970, *Earthquake* **2,** 1–11 (in Chinese).

Liu, H. L. and H. Kanamori (1980). Determination of source parameters of mid-plate earthquakes from waveforms of body waves, *Bull. Seism. Soc. Am.* **70,** 1989–2004.

Ma, X. and D. Wu (1987). Cenozoic extensional tectonics in China, *Tectonophysics* **133,** 243–255.

Ma, Z. (1987). Comparison of continental seismotectonics between eastern China and eastern U.S., *Earthquake Res. in China* **1**(2), 241–251.

Ma, Z., C. Fu, Y. Zhang, C. Wang, Q. Zhang, and D. Liu (1982). *Nine Major Earthquakes of China from 1966 to 1976,* Seismological Press, Beijing (in Chinese).

Molnar, P. (1979). Earthquake recurrence intervals and plate tectonics, *Bull. Seism. Soc. Am.* **69,** 115–133.

Molnar, P. and Q. Deng (1984). Faulting associated with large earthquakes and the average rate of deformation in central and eastern Asia, *J. Geophys. Res.* **89,** 6203–6227.

Nuttli, O. W. (1973). The Mississippi Valley earthquake of 1811 and 1812: intensities, ground motion and magnitudes, *Bull. Seism. Soc. Am.* **63,** 227–248.

Okal, E. A. (1981). Intraplate seismicity of Antarctica and tectonic implications, *Earth Planet. Sci. Lett.* **52,** 397–409.

Qin, D. (1982). On the block faulting and its boundary active fault in the lower Changjiang (Yangtze) River and the related Liyang earthquakes, in *The Active Faults in China,* Committee on Seismogeology (Editor), The Seismological Society of China, 196–199 (in Chinese).

Richardson, R. M. and S. C. Solomon (1976). Intraplate stress as an indicator of plate tectonic driving forces, *J. Geophys. Res.* **81,** 1847–1856.

Satake, K. (1985). Effects of station coverage on moment tensor inversion, *Bull. Seism. Soc. Am.* **75,** 1657–1667.

Scholz, C. H. (1977). A physical interpretation of the Haicheng earthquake prediction, *Nature* **267,** 121–124.

Scott, D. R. and H. Kanamori (1985). On the consistency of moment tensor source mechanisms with first-motion data, *Phys. Earth Planet. Interiors* **37,** 97–107.

Shen, B., D. Zhu, F. Zhu, and N. He (1985). Water radon anomaly of No. 17 well before the M 6.2 earthquake in South Yellow Sea, *Earthquake* **1,** 13–17 (in Chinese).

Stein, S., N. H. Sleep, R. J. Gellor, S. C. Wang, and G. C. Kroeger (1979). Earthquakes along the passive margin of eastern Canada, *Geophys. Res. Lett.* **6,** 537–540.

Sun, S. and S. Zhu (1985). Earthquake recurrence intervals on the South Yellow Sea of China, *J. Seism. Res.* **8(5),** 515–521 (in Chinese).

Sykes, L. (1978). Intraplate seismicity, reactivation of preexisting zones of weakness, alkaline magmatism and other tectonism postdating continental fragmentation, *Rev. Geophys. Space Physics* **16,** 621–688.

Sykes, L. and M. Sbar (1974). Focal mechanism solutions of intraplate earthquakes and stresses in the lithosphere, in *Geodynamics of Iceland and the North Atlantic Area,* L. Kristjansson (Editor), D. Reidel Publishing Co.

Talwani, P. (1986). Seismotectonics of the Charleston region, *Proceedings of the 3rd U.S. National Conference on Earthquake Engineering* **1,** 15–24.

Tapponnier, P. and P. Molnar (1977). Active faulting and tectonics in China, *J. Geophys. Res.* **82,** 2905–2930.

Teng, C., Y. Chang, K. Hsu, and F. Fan (1979). On the tectonic stress field in China and its relation to plate movement, *Phys. Earth Planet. Interiors* **18,** 257–273.

Teng, J.-W., K.-Z. Sun, S.-B. Xiong, H. Yao, Z.-X. Yin, L.-F. Cheng, C.-S. Xue, D.-S. Tian, T.-Y. Hao, M.-H. Lai, and M.-C. Wu (1985). Explosion seismological study for velocity distribution and structure of the crust and upper mantle from Maanshan to Qidong of the southern parts of China, *Acta Geophys. Sinica* **28(2),** 155–169.

Wageman, J. M., T. W. C. Hilde, and K. O. Emery (1970). Structural framework of East China Sea and Yellow Sea, *Am. Assoc. Pet. Geol. Bull.* **54,** 1611–1643.

Wang, X. and Y. Xu (1985). Short-term and impending anomalies of chlorine ion content in the well at Huishan pesticide plant, Wuxi, before the South Yellow Sea earthquake with $M = 6.2$, *Earthquake* **3,** 15–17 (in Chinese).

Xie, Y. (1983). *Compilation of Historical Materials of Chinese Earthquakes,* Vol. 5, Science Press, Beijing (in Chinese).

Xie, Y. and M. Qai (1985) *Compilation of Historical Materials of Chinese Earthquakes,* Vol. 2, Science Press, Beijing (in Chinese).

Zhang, D. and C. He (1986). The M 6.2 Yellow Sea earthquake in Jiangsu Province: its monitoring and prediction, *Earthquake Res. in China* **1**(1), 9–22.

Zhang, Z. M., J. G. Liou, and R. G. Coleman (1984). An outline of the plate tectonics of China, *Geol. Soc. Am. Bull.* **95,** 295–312.

CENTER FOR EARTHQUAKE RESEARCH AND INFORMATION AND
DEPARTMENT OF GEOLOGICAL SCIENCES
MEMPHIS STATE UNIVERSITY
MEMPHIS, TENNESSEE 38118

Manuscript received 15 November 1988